Deep Diffused APDs for Charged Particles Timing Applications

M. Centis Vignali[1], M. Gallinaro[1,2], B. Harrop[3], C. Lu[3], M. McClish[4], K. T. McDonald[3], M. Moll[1], F. M. Newcomer[5], S. Otero Ugobono[1,6], and S. White[1,7]

[1]CERN, Geneva, Switzerland
[2]LIP, Lisbon, Portugal
[3]Princeton University, Princeton, USA
[4]Radiation Monitoring Devices, Watertown, USA
[5]University of Pennsylvania, Philadelphia, USA
[6]Universidade de Santiago de Compostela, Santiago de Compostela, Spain
[7]University of Virginia, Charlottesville, USA

January 29, 2018

Abstract

For their operation at the CERN High Luminosity Large Hadron Collider (HL-LHC), the ATLAS and CMS experiments are planning to implement dedicated systems to measure the time of arrival of minimum ionising particles with an accuracy of about 30 ps. The timing detectors will be subjected to radiation levels corresponding up to a 1-MeV neutrons fluence (Φ_{eq}) of $10^{15}\,\mathrm{cm}^{-2}$ for the goal integrated luminosity of HL-LHC of 3000 fb^{-1}.

In this paper deep diffused Avalanche Photo Diodes (APDs) produced by Radiation Monitoring Devices are examined as candidate timing detectors for HL-LHC applications. To improve the detector's timing performance, the APDs are used to directly detect the traversing particles, without a radiator medium where light is produced. These APDs are operated at 1.8 kV, resulting in a gain of up to 500. The performance of the detectors is evaluated using both laboratory characterisations and beam tests.

Devices with an active area of $8 \times 8\,\mathrm{mm}^2$ and AC-coupled readout were characterised in beam tests. The timing performance as well as the uniformity of response and detection efficiency are examined in this paper.

The effects of radiation damage on current, signal amplitude, noise, and timing of the APDs are evaluated using detectors with an active area of $2 \times 2\,\mathrm{mm}^2$ and DC-coupled readout. These detectors were irradiated with neutrons up to $\Phi_{eq} = 10^{15}\,\mathrm{cm}^{-2}$. Their timing performance was characterised using a pulsed infrared laser.

Contents

1 Introduction

The high luminosity upgrade of the CERN Large Hadron Collider (HL-LHC) foreseen to start in 2026 will provide an instantaneous luminosity of $5 \cdot 10^{34}\,\mathrm{cm}^{-2}\mathrm{s}^{-1}$ with a bunch spacing of 25 ns, and an average pile-up of 200 collisions per bunch crossing [1]. To reduce the effects of pile-up on the physics analyses, both the ATLAS and CMS experiments are planning to implement dedicated systems to measure the time of arrival of minimum ionising particles (MIPs) with an accuracy of about 30 ps. These systems include both scintillators coupled to photo-detectors and silicon detectors. By providing the time of arrival information of MIPs, these systems allow for the correct association of particles to their primary vertexes in the case where the latter have a proximity in space that renders their separation impossible. An improved time of arrival resolution would also effectively reduce the vertex density, and improve the vertex reconstruction capability of the experiments. These timing detectors will be subjected to radiation levels corresponding to a 1-MeV neutrons fluence (Φ_{eq}) of up to $10^{15}\,\mathrm{cm}^{-2}$ for the goal integrated luminosity of HL-LHC of $3000\,\mathrm{fb}^{-1}$.

This paper summarises the characterisation of deep-diffused Avalanche Photo Diodes (APDs) produced by Radiation Monitoring Devices [2] used as timing detectors for charged particles. The timing performance as well as the radiation hardness of these devices are addressed. Section 2 provides a general description of the deep diffused APDs. In section 3 a detailed description of the devices used in this study is given. Section 4 reports the characterisation of neutron-irradiated APDs with an active area of $2 \times 2\mathrm{mm}^2$. Sections 5 and 6 respectively summarise uniformity and timing measurements of APDs with an active area of $8 \times 8\mathrm{mm}^2$ with DC-coupled readout. Section 7 describes the methods and results obtained though beam tests of APDs with an active area of $8 \times 8\mathrm{mm}^2$ with AC-coupled readout. Finally, section 8 summarises the results obtained in this study.

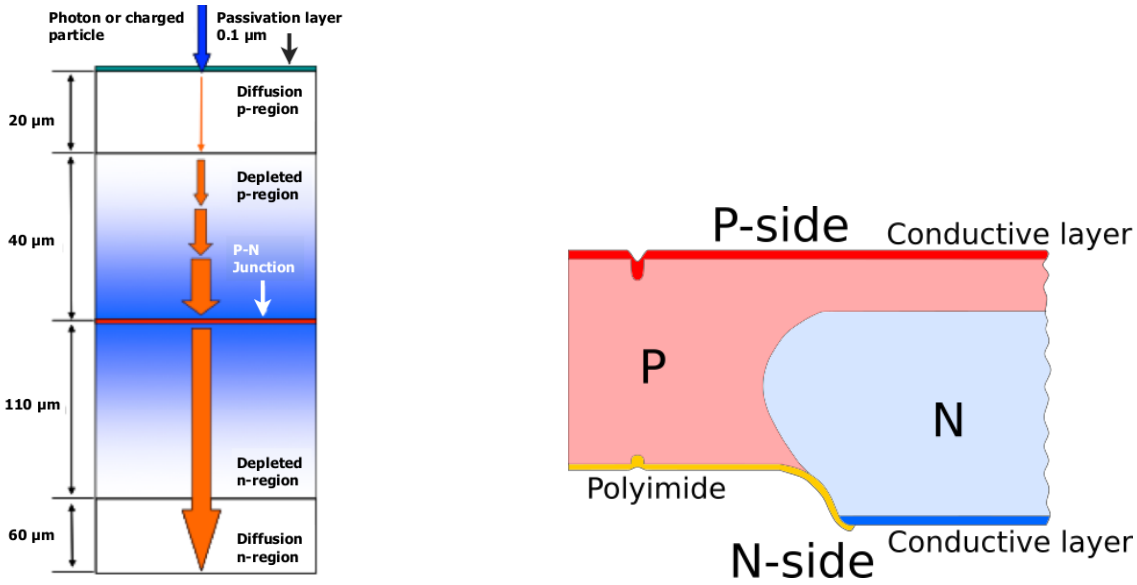

Figure 1: Schematic cross-sections of a deep diffused APD. **Left:** centre of the detector. The thickness of the depleted region corresponds to a bias voltage of 1.8 kV. **Right:** detector edge.

2 Deep Diffused APDs

Deep diffused APDs consist of a pn-junction operated in reverse bias. Bias voltage is applied to the detector in order to achieve an electric field high enough for the charge carriers to undergo impact ionisation. This mechanism is responsible for the multiplication of the charge carriers released by the passage of a charged particle or light impinging on the detector.

The pn-junction is located several tens of microns from the detector surface. This, together with the shape of the doping profile, prevents the depletion region from reaching the detector's surface, avoiding breakdown and noise due to surface effects. The concept of full depletion voltage, usually applied to detectors produced through the planar process, is not used with this kind of APDs.

The occurrence of breakdown and noise from the edges of the detector die is mitigated by reducing the electric field in these positions. This can be achieved by beveling the detector's edges [3]. Another way to reduce the electric field at the edges of the depletion region is to distribute the doping in the sensor such that the depletion region is "bent" and terminated on one of the sensor's surfaces [3]. A mesa structure can be used to reduce the electric field.

Deep diffused APDs get their name from the process used to produce a pn-junction several tens of microns from the detector surface. The APDs used in this work are produced on silicon using the method explained in [3, 4]. Grooves are carved on both sides of an n-doped silicon wafer and p-type dopants are diffused into the silicon. The grooves run parallel to the future die edges and shape the distribution of the p-type dopants into the silicon. This process results into an n-doped region enclosed by the p-doped silicon. The wafer is ground on one side to reach the n-doped region. The n-doped region is exposed on one side and surrounded by p-type silicon. The pn-junction runs parallel to the detector surface and curves toward the side with the exposed n-doped region. Non-metallic conductive layers are added on both sides to provide ohmic contacts to the p and n-doped volumes. A mesa structure is then etched following the pn-junction on the side where the n-doped region is exposed. Finally, Polyimide is deposited around the mesa structure and the wafer is diced.

Schematic cross-sections of the centre and the edge of the resulting device are shown in figure 1. In the following, the faces of the detectors will be referred to as p- and n-side, according to the sketch shown in figure 1. The applied bias voltage is usually around 1.8 kV, resulting in a gain of

up to 500. At this bias voltage the thickness of the depletion region is around 150 μm.

3 Samples and Irradiations

All the APDs used in this study present the structure detailed in the previous section. Detectors of two different sizes were used. In this section, the geometry and readout of the different APDs are explained.

3.1 2×2 mm^2 APDs

APDs with a nominal active area of 2×2 mm^2 were used to study the effects of neutron irradiation. The dies of these devices have an area of 3.1×3.1 mm^2 and a circular mesa structure with a diameter of about 0.8 mm. These devices are mounted on ceramic supports, two metallic leads are used to contact the p- and n-sides of the detector. The n-side of the detector faces the ceramic support. The contact between the APD and the metal leads is achieved using conductive glue.

The 2×2 mm^2 APDs have a DC-coupled readout. In order to facilitate the handling and electrical connection to the sensors, each APD was mounted on a printed circuit board (PCB) for its characterisation both before and after irradiation. The PCB was equipped with a temperature sensor and the connectors needed to link the APD to the measuring devices.

The sensors were irradiated with neutrons at the nuclear reactor of the Jožef Stefan Institute in Ljubljana [5]. The fluences accumulated by the sensors ranged from $\Phi_{eq} = 3 \cdot 10^{13}\,\mathrm{cm}^{-2}$ to $\Phi_{eq} = 10^{15}\,\mathrm{cm}^{-2}$. Neither bias nor cooling were applied during the irradiation. After irradiation, the samples were stored at a temperature below -18°C to avoid the annealing of the defects produced during irradiation.

3.2 8×8 mm^2 APDs

APDs with a nominal active area of 8×8 mm^2 were characterised in several beam tests. The dies of these devices have an area of 10×10 mm^2 and a square mesa structure with 7.5 mm sides.

Studies similar to the one reported in section 5 shown that the amplitude of the signal produced by the sensor when illuminated by a laser depends on the distance between the point in which the sensor is struck by the laser and the point where the sensor is connected to the readout electronics. This behaviour is the result of the non-negligible resistance of the conducting layers applied to the p- and n-side of the detector.

Two methods were used to improve the uniformity of response. The first one, used in the devices characterised in beam tests, relies on an AC-coupled readout of the p-side of the detector. A gold layer is applied to the n-side of the detector to improve its conductivity. The electrical contact to the p-side is achieved through the formation of a bond-pad and wire-bonding. The p-side is covered by a Kapton layer and a metallic mesh is placed above the Kapton. The mesh picks-up the signal and provides an electrical path with a resistivity lower than the one of the conductive layer. The sensors produced with this configuration were usually placed on PCBs containing the readout electronics.

Another method used to improve the uniformity of response is the metallisation of both the p- and n-side of the detector. The metallisation consists in an aluminium deposition. The detectors produced with this configuration have a DC-coupled readout and were used in laboratory tests. These sensors were mounted on the same PCBs as the 2×2 mm^2 APDs, that contain a temperature sensor and the connectors to bias and readout the sensor.

4 Laboratory Characterisation of Irradiated 2×2 mm^2 APDs

4.1 Experimental Methods

Two experimental setups were used to characterise the APDs.

The current-voltage characteristic of the detectors was measured using a voltage source and a picoammeter connected in series to the sensor under test. The sensor was placed inside a climate chamber flushed with dry air where the temperature could be controlled. The temperature sensor on the PCB was used to ensure that the APD reached thermal equilibrium with the air in the climate chamber before starting the measurements.

The response of the APDs to a pulsed infrared laser was measured in a different setup and used to determine the variation of the sensor's signal and time resolution as a function of bias voltage and irradiation fluence. The laser has a wavelength of 1064 nm and the pulses have a duration of 200 ps. The repetition rate was chosen to be 200 Hz. The intensity of the light impinging on the APD was determined to correspond to a charge deposition in the sensor of 15 or 0.8 MIPs per pulse, depending on the measurement. A shutter is used to change the light intensity. The amount of deposited charge per laser pulse was measured using a non-irradiated pad diode of known thickness. The charge deposited for one MIP is defined as 74 electron hole pairs per micron of silicon. The wavelength used has an absorption length in silicon of about 1 mm, resulting in the generation of electron hole pairs through the whole sensor thickness. The light pulses are propagated from the laser to the sensor through an optical fibre. A coupler diverts part of the light to a photodiode that is used to monitor the intensity of the light pulses. An optical system focuses the light on the sensor surface producing a beam spot of about 15 μm in diameter. The bias voltage of the sensor under test is provided by a voltage source containing a picoammeter used to monitor the current flowing through the sensor. The temperature of the APD was controlled using a cooling system constituted by a Peltier element and a chiller. The temperature measured by the temperature sensor on the PCB was used as input to the Peltier control system. The APD was housed in a light-tight Faraday cage flushed with dry air during the measurements. The APD signal was amplified using a CIVIDEC C2HV broadband amplifier [6]. Both the signals of the APD and the photodiode were digitised using an oscilloscope with 2.5 GHz bandwidth and a sampling rate of 20 GSa/s.

For the measurement of the APD signal amplitude and uniformity of response, an amplification of 10 dB was used, together with a light intensity corresponding to 15 MIPs. This amplification was achieved by attenuating the APD signal with a 30 dB attenuator and then amplifying it with a 40 dB amplifier. The 40 dB amplifier is the same used in the time resolution measurements. The reduction of the gain to 10 dB is necessary in order to perform the amplitude measurements over the desired bias voltage range while remaining in the amplifier's linear range. For each measurement condition, the waveforms were averaged 256 times in the oscilloscope before being stored for analysis.

The time resolution measurements were performed applying a 40 dB amplification to the APD signal. No averaging was applied to the waveforms. A gain of 40 dB provides a better signal to noise ratio for the APD signal, compared to the 10 dB used for the amplitude measurement. The intensity of the light shone on the APDs for these measurements corresponded to 0.8 MIPs. The optical system was modified for the timing measurements. A splitter and delay line system was introduced, allowing to shine two light pulses on the sensor for each pulse generated by the laser. The system is realised using optical fibre, and consisted of a splitter, a short and a long optical fibre branch, and a merger. The difference in length between the two branches corresponds to a delay of 50 ns between the pulses. The sensor's signals from the light pulses were digitised in the same waveform in the oscilloscope. The difference in the amplitude of the two signals was below 5%. Given the similar amplitude, the signals can be used to determine the time resolution of the detector under test, without the need of an external timing reference.

The APD temperature was -20°C during all measurements reported in this section. For the measurements of intensity as a function of bias voltage and the timing measurements using the laser, the light was shone on the centre of the APDs.

4.2 Results

Current-voltage characteristic The current-voltage (IV) characteristic of the APDs is shown, for different fluences, in figure 2. Before irradiation, below 1600 V, the current assumes a value of

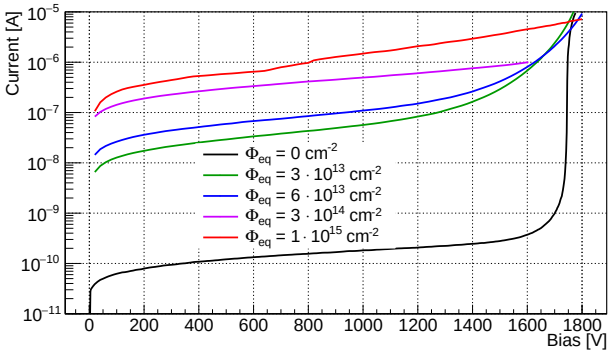

Figure 2: Current-voltage characteristics of the APDs measured at $-20°$C for different fluences.

less than a few nA. In this region the main contribution to the current is thought to be surface current. Between 1600 and 1800 V, the current increases by 4 orders of magnitude. This is the region where the multiplication dominates the IV characteristic of the non-irradiated sensors. The surface current is not affected by multiplication, therefore the multiplication of bulk current in the non-irradiated sensors can not be seen in the IV curve until the gain is sufficiently high.

The irradiation enhances the bulk generation current of the devices, as can be seen in the region between 0 and 1200 V, where the gain of the sensors does not influence the curves. As the bulk current is amplified, the shape of the irradiated sensors' curves is different from that of the non-irradiated sensor. The change in the magnitude of the current at high voltages is different with respect to the non-irradiated sensor, suggesting that the gain of the detectors is reduced by irradiation, or respectively that a higher bias voltage is required to obtain the same gain as for the non-irradiated sensor.

The sensor irradiated to $\Phi_{eq} = 3 \cdot 10^{14}\,\mathrm{cm}^{-2}$ shows a breakdown around 1600 V, therefore no information about its IV characteristic is available at higher bias voltages. This also applies to the amplitude measurements presented below.

Uniformity of response The uniformity of response was measured using an infrared laser with pulses with an intensity corresponding to 15 MIPs and an amplification of 10 dB. The laser was focused on different parts of the sensors and the average of 256 waveforms was stored and the signal amplitude extracted. The signal amplitude as a function of position of the laser spot on the sensors is shown in figure 3. The difference in the bias voltage applied to the detectors is due to the current drawn by the detectors under bias. The biasing and readout circuit had a total resistance of 13 MΩ connected in series to the sensor under test. The bias voltage applied to the readout circuit was 1700 V for all samples, the difference in voltage from this value are due to the potential drop caused by the sensors' dark current flowing through the 13 MΩ load. All the values of bias voltage presented in the following take into account this effect.

The sensor irradiated to $\Phi_{eq} = 3 \cdot 10^{14}\,\mathrm{cm}^{-2}$ could be biased at a higher voltage with respect to the IV measurement. This is probably a consequence of the annealing of the radiation damage of the detector, since the measurement shown in figure 3 were performed after the current-voltage and amplitude measurements. This suggests that the annealing status of the detectors can influence their breakdown behaviour.

The amplitude is higher at lower x values, regardless of the fluence. This effect, although not fully understood for these devices, is thought to be similar in origin to the one studied in section 5 for APDs with an active area of 8×8 mm^2. In each plot of figure 3, a circular region with increased amplitude is present. This region corresponds to the mesa structure in the back of the devices. Part of the light from the laser is reflected from the curved surface of the mesa toward the active area of the detectors, resulting in an increased signal. The sensitive area of the detectors is affected by irradiation. However, the response of the detectors appears uniform close

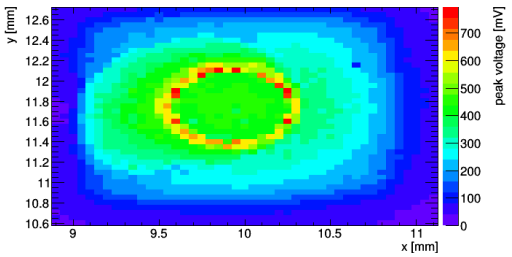

(a) $\Phi_{eq} = 0\,\mathrm{cm}^{-2}$, 1700 V

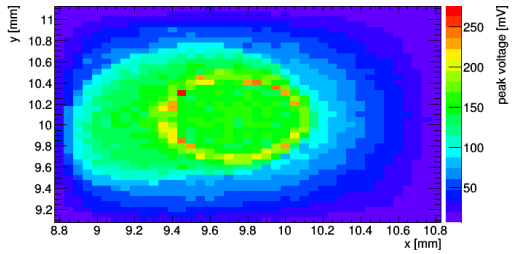

(b) $\Phi_{eq} = 3 \cdot 10^{13}\,\mathrm{cm}^{-2}$, 1679 V

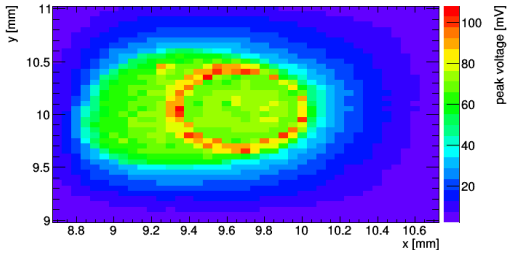

(c) $\Phi_{eq} = 6 \cdot 10^{13}\,\mathrm{cm}^{-2}$, 1673 V

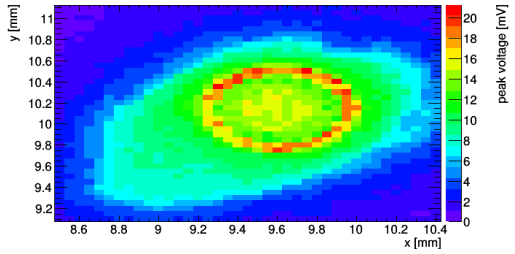

(d) $\Phi_{eq} = 3 \cdot 10^{14}\,\mathrm{cm}^{-2}$, 1677 V

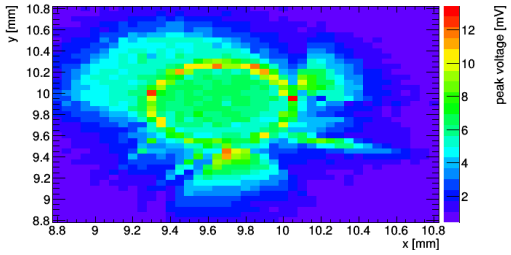

(e) $\Phi_{eq} = 10^{15}\,\mathrm{cm}^{-2}$, 1644 V

Figure 3: Signal amplitude as a function of the position where the laser was focused on the sensors measured at $-20°$C. The laser intensity corresponds to 15 MIPs. An amplification of 10 dB was used.

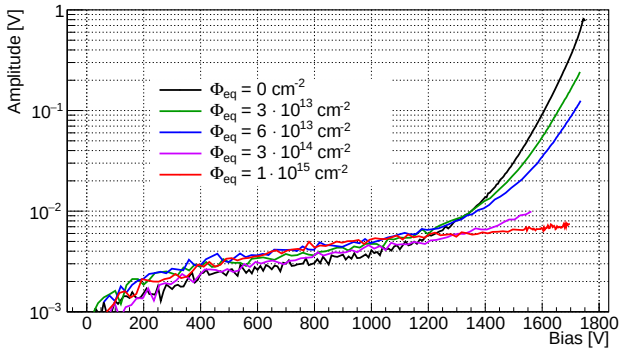

Figure 4: Amplitude of the APDs signal as a function of bias voltage and fluence measured at $-20°$C. The laser intensity corresponds to 15 MIPs. An amplification of 10 dB was used.

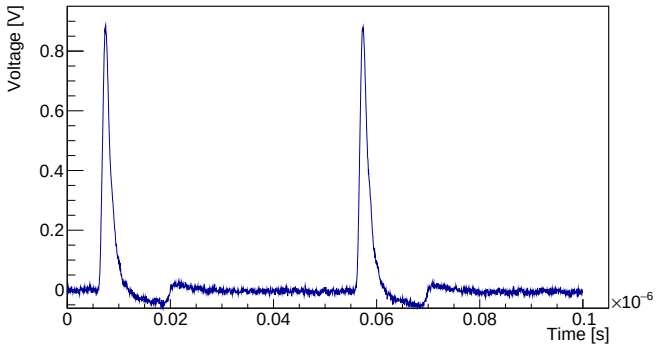

Figure 5: Waveform from a non-irradiated 2×2 mm^2 APD biased at 1665 V operated at $-20°$C. The laser intensity corresponds to 0.8 MIPs. An amplification of 40 dB was used.

to the detector centre, in the area enclosed by the mesa structure. The measurements shown in the rest of this section were performed by shining the light in the centre of the detectors.

Signal amplitude The amplitude was measured from the baseline of the pulse, calculated using the part of the waveform preceding the laser pulse. The results are shown in figure 4 as a function of bias voltage and fluence.

The measured amplitudes present similar values up to 1200 V, for all the fluences. For voltage values above 1200 V, the signal amplitude decreases with increasing fluence, indicating a reduction of the gain for the irradiated detectors. The behaviour of the detectors indicates that for fluences at least up to $\Phi_{eq} = 6 \cdot 10^{13}$ cm^{-2} the gain of the detectors could be recovered by applying a higher bias voltage.

Time resolution The time resolution of the sensors was determined using an infrared laser focused on the detector centre. An optical system was used to have two light pulses shine on the sensor under test for each pulse produced by the laser. A waveform corresponding to one laser pulse is shown in figure 5. The amplification used for the time resolution measurements was 40 dB, and no averaging was applied to the waveforms. 2000 waveforms were acquired for each measurement condition.

The average signal amplitude as a function of bias voltage and fluence is shown in figure 6. The amplitude is limited by two components of the experimental setup. The limiting factor for the non-irradiated sensor is the amplifier, that has a linear region corresponding to an output amplitude of

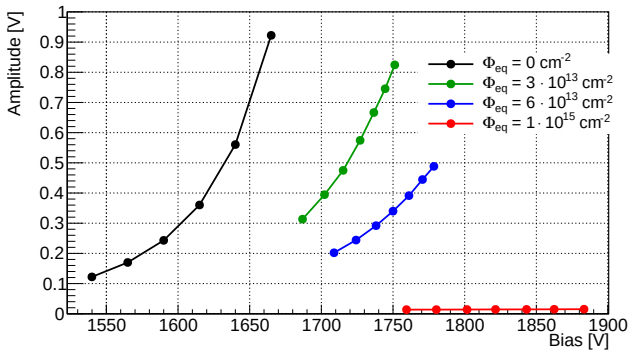

Figure 6: Average amplitude of the 2×2 mm^2 APDs signal as a function of bias voltage and fluence measured at -20°C. The laser intensity corresponds to 0.8 MIPs. An amplification of 40 dB was used.

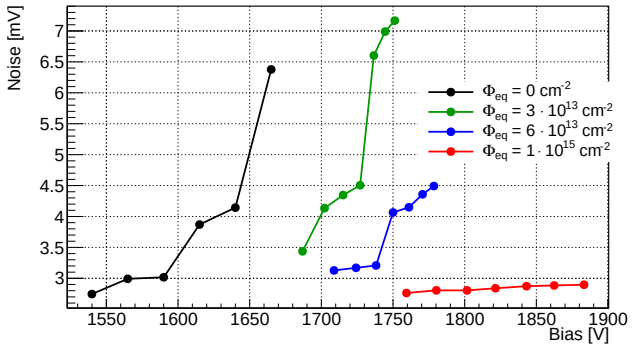

Figure 7: 2×2 mm^2 APDs' noise as a function of bias voltage and fluence measured at -20°C. An amplification of 40 dB was used.

± 1 V. For the irradiated sensors, the maximum current provided by the high voltage power supply was reached, limiting the gain achieved by the devices. The difference between the amplitude of the two signal peaks present in each waveform was less than 5% for each measurement. The time resolution of the sensor irradiated to $\Phi_{eq} = 3 \cdot 10^{14}\,\mathrm{cm}^{-2}$ was not measured due to its breakdown behaviour that poses a risk to the electronics used in these measurements.

The noise is defined as the standard deviation of the distribution of the waveform points around the baseline, for the portion of the waveform preceding the pulse due to laser illumination. The noise of the APDs, as a function of bias voltage and irradiation fluence, is shown in figure 7. The noise of the APDs with $\Phi_{eq} \leq 6 \cdot 10^{13}\,\mathrm{cm}^{-2}$ shows a stronger dependence on the applied bias voltage than the the detector irradiated to $\Phi_{eq} = 10^{15}\,\mathrm{cm}^{-2}$. This suggests that the multiplication mechanism affects the noise of the sensors.

The signal to noise ratio (SNR) is defined as the ratio between amplitude and noise and is shown in figure 8. The SNR is not a monotone function of the applied bias voltage. The sensor irradiated to $\Phi_{eq} = 10^{15}\,\mathrm{cm}^{-2}$ shows a weaker dependence of SNR on bias voltage than the other sensors. This is attributed to the lower value of gain of this sensor compared to the others.

The average 20%-to-80% rise time of the sensors is shown in figure 9. The crossing time of the 20% and 80% thresholds was determined using a linear interpolation between two points of the waveform. The values for the sensor irradiated to $\Phi_{eq} = 10^{15}\,\mathrm{cm}^{-2}$ lie between 5.1 and 5.3 ns and are not shown since they are affected by its lower SNR, that spoils the determination of the 20% point. The rise time increases with increasing bias voltage. The difference between the rise time of the sensors lies within 11%, the rise time does not seem to be affected by irradiation.

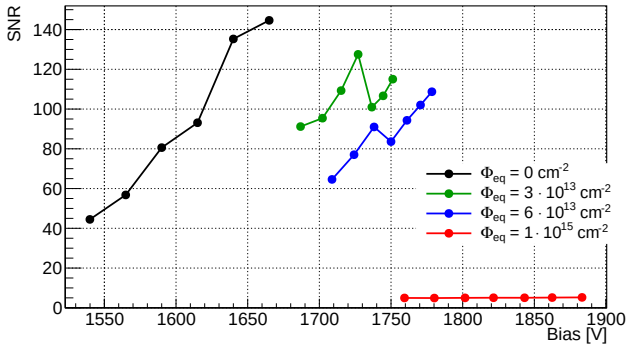

Figure 8: Signal to noise ratio of the 2×2 mm^2 APDs as a function of bias voltage and fluence measured at -20°C. The laser intensity corresponds to 0.8 MIPs. An amplification of 40 dB was used.

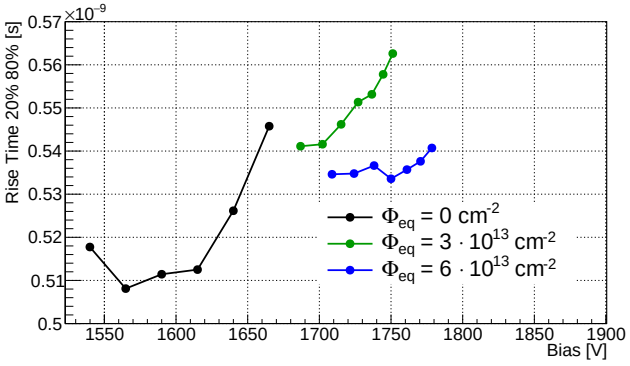

Figure 9: 20%-to-80% rise time of the 2×2 mm^2 APDs signal as a function of bias voltage and fluence measured at -20°C. The laser intensity corresponds to 0.8 MIPs. An amplification of 40 dB was used.

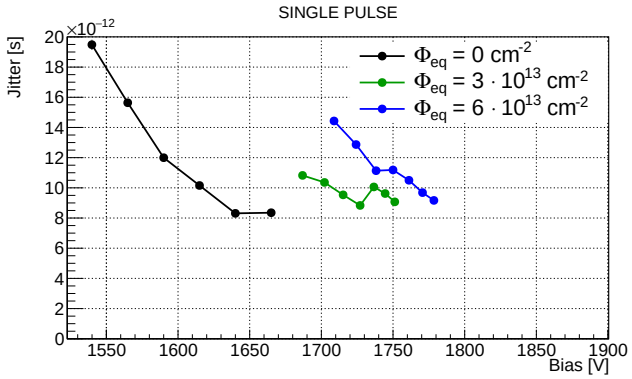

Figure 10: Single pulse time resolution of the 2×2 mm^2 APDs as a function of bias voltage and fluence measured at -20°C. The laser intensity corresponds to 0.8 MIPs. An amplification of 40 dB was used.

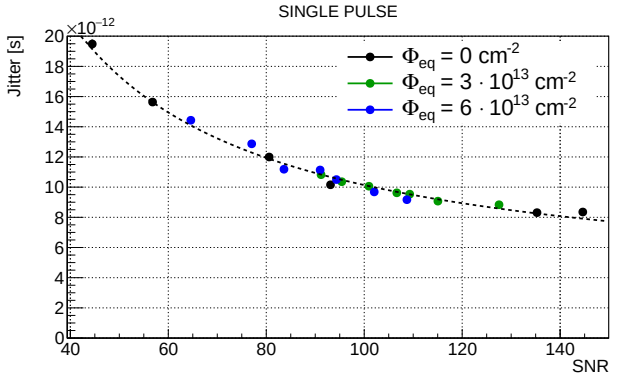

Figure 11: Single pulse time resolution of the 2×2 mm^2 APDs as a function of signal to noise ratio and fluence measured at -20°C. The laser intensity corresponds to 0.8 MIPs. An amplification of 40 dB was used.

The time resolution of the sensors was determined using the two pulses acquired in each waveform. The waveforms are divided in two parts of 50 ns each. The pulses are analysed independently. The time difference between the pulses is calculated using a constant fraction discriminator (CFD) algorithm. This algorithm was chosen since it allows to study the effect of different thresholds applied to the pulses with relative ease, without having to account for the pulse amplitude. The thresholds applied to the pulses were optimised for each measurement condition, choosing the combination that resulted in the best time resolution. The time resolution is defined as the standard deviation of the distribution of the time difference (Δt) between the pulses. The crossing time of the thresholds was determined using a linear interpolation between two points of the waveform. Since the difference in the amplitude of the pulses measured in the same waveform was less than 5%, the time jitter of the sensor and readout electronics for a single pulse (or single pulse time resolution) can be calculated by dividing the two pulses time resolution by $\sqrt{2}$. The single pulse time resolution of the detectors is shown in figure 10 as a function of bias and fluence. The jitter of the sensor irradiated to $\Phi_{eq} = 10^{15}\,\mathrm{cm}^{-2}$ lies between 508 and 553 ps. These values are not shown in the figure for clarity. The other sensors show a trend of decreasing jitter as a function of bias voltage. The behaviour is however not monotonous.

The jitter is found to scale approximately as 1/SNR. Figure 11 shows the jitter as a function of SNR. The dashed line represents a 1/SNR behaviour.

The jitter of the sensors is not degraded by the neutron-induced radiation damage corresponding to a fluence of at least $\Phi_{eq} = 6 \cdot 10^{13}\,\mathrm{cm}^{-2}$. This result is expected to hold for timing

measurements of charged particles. The overall resolution is however expected to worsen due to the fluctuations of the amount of charge deposited per unit length along the particle path. These fluctuations, also known as *Landau noise* [7], can influence the leading edge of the sensor's signal and therefore worsen the time resolution.

5 Uniformity Study of 8×8 mm^2 APDs using an Infrared Laser

The uniformity of response of the 8×8 mm^2 APDs was studied using an infrared laser. The amplitude and integrated signal are shown in figure 12 as a function of the position were the laser illuminated the detector. The sensor was contacted using opaque conductive paint. The point of contact can be seen at the coordinate (4.5, 6) mm. Since the absorption length of the light used in the measurements is greater than the sensor thickness, several features of the surface below the sensor can be seen in the figure. The square mesa structure and the conductive paint used to glue the detector to the PCB used for the measurements can be seen as areas of increased amplitude and signal integral due to their reflection of the light toward the sensor. The PCB has a hole below the detector centre, that results in decreased values of amplitude and signal integral. Since the signal amplitude is affected by both the deposited charge in the detector and the detector properties, the amplitude was normalised using the integrated signal in order to mitigate the former effect. The ratio between the amplitude and the integrated signal is shown in figure 12. The effects of the surface below the sensor are reduced and a dependency of the ratio between amplitude and charge on the distance between the laser spot and the point where the signal is collected from the sensor can be seen. The amplitude of the signal decreases with increasing distance from the electrical contact. This effect is attributed to the non-negligible resistivity of the conductive layers applied to the detector. The dependency of the signal amplitude on the detector position can result in a worsened time resolution.

The two approaches taken to reduce this source of non-uniformity are described in section 3. The results obtained with the AC-coupled mesh readout are shown in section 7. The DC-coupled metallisation resulted in a difference in the ratio between amplitude and charge of less than 2% over a distance of 7 mm between the points illuminated by the laser. No dependency on the distance between illumination and electrical contact was observed. This measurement was performed on a sensor biased to 1800 V at a temperature of 20°C. The metallisation was performed at the clean room facility of CMi-EPFL [8]. The structure consists of an aluminium grid on the n-side and a continuous aluminium layer with an opening at the detector centre on the p-side of the detector. This configuration allows the illumination of the detector centre without reflections.

6 Timing Performance of 8×8 mm^2 APDs using an Infrared Laser

The time resolution of the metallised 8×8 mm^2 APDs with DC-coupled readout was studied using the same setup and procedure used for the characterisation of the irradiated 2×2 mm^2 APDs in section 4. A light intensity corresponding to 0.8 MIPs and an amplification of 40 dB were used. The light was shone in the centre of the detector. The signal amplitude and noise are shown in figure 13 and 14, respectively. The signal amplitude is smaller than the one of the 2×2 mm^2 devices shown in section 4. This can be a consequence of a lower gain of the device under test or the bigger capacitance of the device. The noise is also smaller than the one of the 2×2 mm^2 devices. Both signal amplitude and noise increase as a function of bias voltage.

The 20%-to-80% rise time of the signal is shown in figure 15. The values are bigger than the ones of the 2×2 mm^2 devices. This is a consequence of the bigger sensor capacitance.

The jitter was calculated with the same procedure presented in section 4. The jitter decreases with increasing bias voltage and is found to scale with a 1/SNR behaviour.

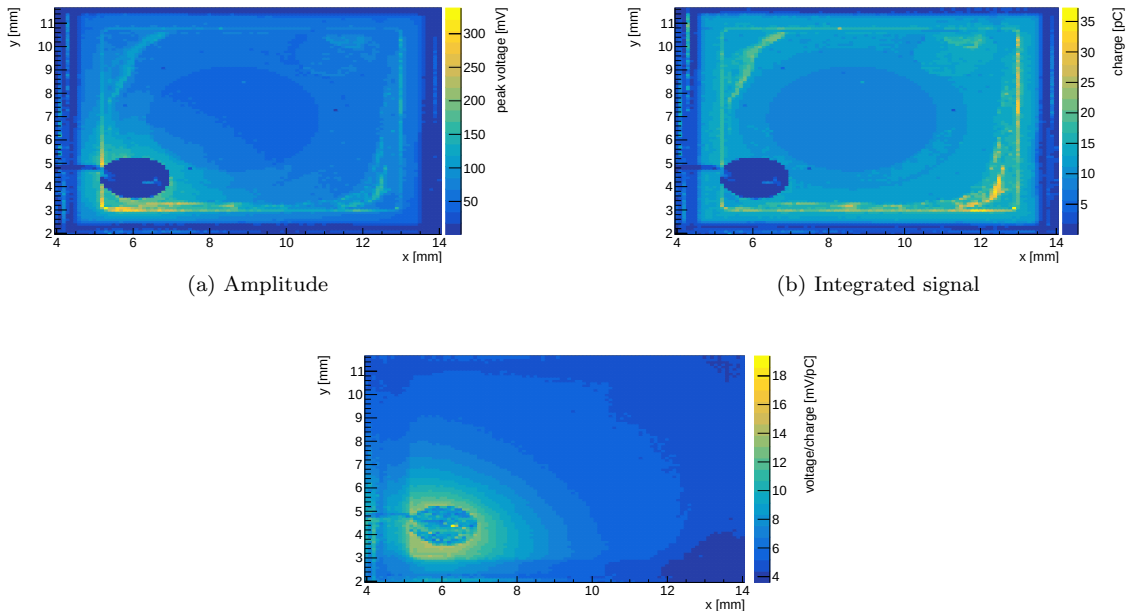

(a) Amplitude

(b) Integrated signal

(c) Ratio

Figure 12: Signal amplitude **(a)**, integral **(b)**, and ratio between amplitude and integral **(c)** of a 8×8 mm^2 APD as a function of position. The sensor was biased at 1700 V, at a temperature of -20°C. The laser intensity corresponds to 15 MIPs. An amplification of 10 dB was used.

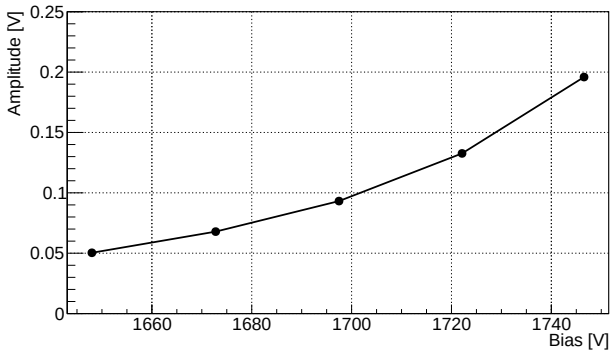

Figure 13: Average amplitude of the metallised 8×8 mm^2 APD signal as a function of bias voltage measured at 20°C. The laser intensity corresponds to 0.8 MIPs. An amplification of 40 dB was used.

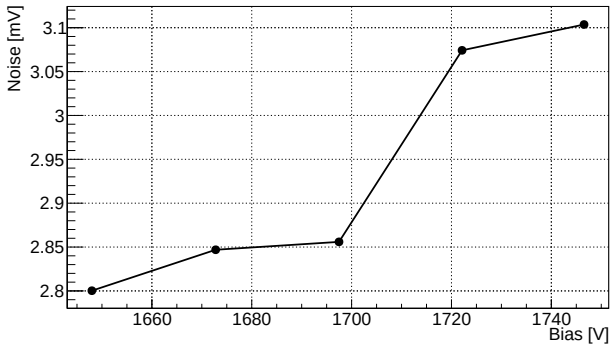

Figure 14: 8×8 mm^2 APD's noise as a function of bias voltage measured at 20°C. An amplification of 40 dB was used.

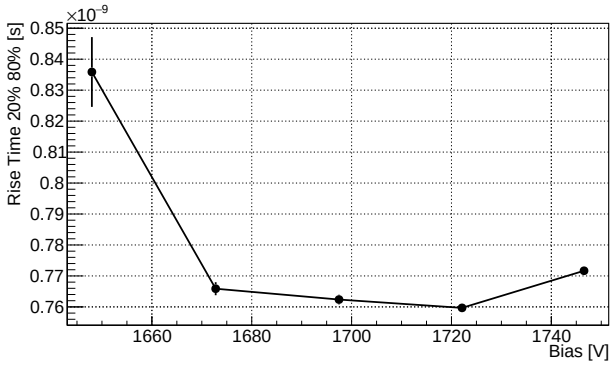

Figure 15: 20%-to-80% rise time of the metallised 8×8 mm^2 APD signal as a function of bias voltage measured at 20°C. The laser intensity corresponds to 0.8 MIPs. An amplification of 40 dB was used.

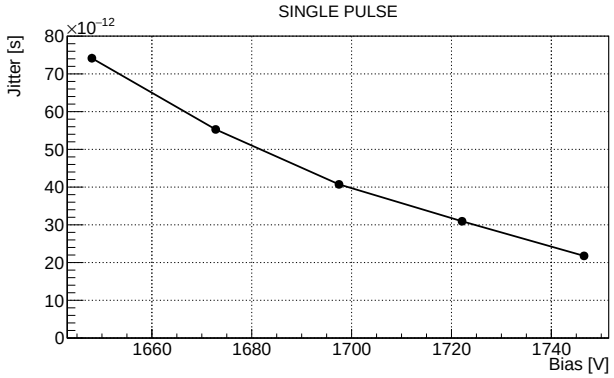

Figure 16: Single pulse time resolution of the metallised 8×8 mm^2 APDs as a function of bias voltage measured at 20°C. The laser intensity corresponds to 0.8 MIPs. An amplification of 40 dB was used.

The metallised 8×8 mm^2 APDs often did not allow for a stable operation when biased above 1700 V. The source of the instability is under investigation. This instability influenced the choice of values of bias voltage used in this section.

7 Beam Tests of 8×8 mm^2 APDs with Mesh Readout

7.1 Setup

7.2 Data Analysis

7.3 Results

8 Summary

Acknowledgments

The work summarised in this paper has been performed within the framework of the RD50 collaboration. This project has received funding from the European Union's Horizon 2020 Research and Innovation programme under Grant Agreement no. 654168. The authors wish to thank J. Bronuzzi for the help during the clean room operations and in the development of the recipe for the metallisation of the devices.

References

[1] HiLumi LHC Collaboration, "HL-LHC Preliminary Design Report." `http://hilumilhc.web.cern.ch/science/deliverables`, 2014.

[2] Radiation Monitoring Devices Inc. 44 Hunt St. Watertown USA, `http://rmdinc.com/`.

[3] M. McClish, R. Farrell, F. Olschner, M. R. Squillante, G. Entine, and K. S. Shah, "Characterization of very large silicon avalanche photodiodes," in *IEEE Symposium Conference Record Nuclear Science 2004.*, vol. 2, pp. 1270–1273 Vol. 2, Oct 2004.

[4] R. Farrell and K. Vanderpuye, "Large area semiconductor detector with internal gain," Sept. 11 2007. US Patent 7,268,339.

[5] L. Snoj, G. Žerovnik, and A. Trkov, "Computational analysis of irradiation facilities at the jsi triga reactor," *Applied Radiation and Isotopes*, vol. 70, no. 3, pp. 483 – 488, 2012.

[6] CIVIDEC Instrumentation GmbH. Schottengasse 3A Wien Austria, `http://cividec.at/`.

[7] N. Cartiglia et al., "Tracking in 4 dimensions," *Nuclear Instruments and Methods in Physics Research Section A: Accelerators, Spectrometers, Detectors and Associated Equipment*, vol. 845, pp. 47 – 51, 2017. Proceedings of the Vienna Conference on Instrumentation 2016.

[8] CMi-EPFL. CH-1015 Lausanne, `https://cmi.epfl.ch/`.